THE FASEB JOURNAL • RESEARCH • www.fasebj.org

FFAR2-FFAR3 receptor heteromerization modulates short-chain fatty acid sensing

Zhiwei Ang,* Ding Xiong,*,† Min Wu,*,†,‡ and Jeak Ling Ding*,1

*Department of Biological Sciences, Faculty of Science, †Centre for Bioimaging Sciences, and ‡Mechanobiology Institute, National University of Singapore, Singapore

ABSTRACT: Free fatty acid receptors 2 and 3 (FFAR2/FFA2/GPR43 and FFAR3/FFA3/GPR41) are mammalian receptors for gut microbiota–derived short-chain fatty acids (SCFAs). These receptors are promising drug targets for obesity, colitis, colon cancer, asthma, and arthritis. Here, we demonstrate that FFAR2 and FFAR3 interact to form a heteromer in primary human monocytes and macrophages *via* proximity ligation assay, and during heterologous expression in HEK293 cells *via* bimolecular fluorescence complementation and fluorescence resonance energy transfer. The FFAR2-FFAR3 heteromer displayed enhanced cytosolic Ca^{2+} signaling (1.5-fold increase relative to homomeric FFAR2) and β-arrestin-2 recruitment (30-fold increase relative to homomeric FFAR3). The enhanced heteromer signaling was attenuated by FFAR2 antagonism (CATPB), $G_{\alpha q}$ inhibition (YM254890), or $G_{\alpha i}$ inhibition (pertussis toxin). Unlike homomeric FFAR2/3, the heteromer lacked the ability to inhibit cAMP production but gained the ability to induce p38 phosphorylation in HEK293 and inflammatory monocytes *via* a CATPB- and YM254890-sensitive mechanism. Our data, taken together, reveal that FFAR2 and FFAR3 may interact to form a receptor heteromer with signaling that is distinct from the parent homomers—a novel pathway for drug targeting.—Ang, Z., Xiong, D., Wu, M., Ding, J. L. FFAR2-FFAR3 receptor heteromerization modulates short-chain fatty acid sensing. FASEB J. 32, 289–303 (2018). www.fasebj.org

KEY WORDS: GPCR heteromer · FFA2/GPR43 · FFA3/GPR41

Free fatty acid receptors 2 and 3 [FFAR2 (also known as FFA2 or GPR43) and FFAR3 (also known as FFA3 or GPR41)] are GPCRs that are expressed on mammalian cells. The expression of FFAR2 and FFAR3 allows mammalian cells to sense the presence of microbiota-derived short-chain fatty acids (SCFAs) such as acetate, butyrate, and propionate (EC_{50} of ~0.5 mM) (1, 2). The genetic deletion of either FFAR2 or FFAR3 expression in mice was found to either exacerbate or reduce a number of inflammatory diseases. Studies have implicated FFAR2 in diabetes (3), obesity (4–9), colitis (10–16), colon cancer (17), and arthritis (10); FFAR3 has been implicated in diabetes (3), colitis (14), hypertension (18), and asthma (19).

The pharmacologic modulation of FFAR2/3 to treat the many FFAR2/3-associated diseases is currently being explored but is focused exclusively on targeting FFAR2 or FFAR3 individually (20). As exemplified by the heteromer of the D_1-D_2 dopamine (21, 22), GPCRs may interact to form heteromers that display signaling that is distinct from the parent homomers (23–25). Such GPCR heteromers are potential drug targets. For example, a peptide drug designed to specifically disrupt D_1-D_2 dopamine heteromer has been shown to act as an antidepressant (26). A putative FFAR2-FFAR3 heteromer may mediate the disease phenotypes observed in FFAR2/3 single-knockout studies (3–20) because the knockout of either FFAR2 or FFAR3 would lead to the loss of the heteromer and any heteromer-dependent functions.

A prerequisite to FFAR2-FFAR3 heteromer formation is the coexpression of FFAR2 and FFAR3 within the same cell. In human and mouse pancreatic β-cell lines, the coexpression of FFAR2 and FFAR3 can be inferred from the recovery in insulin secretion upon the small interfering RNA (siRNA)-mediated knockdown of either receptor (3). Coexpression was also detected *via* immunohistochemistry (IHC) in colon epithelial cells (human and mouse), human monocytes, and human macrophages (27–29). In

ABBREVIATIONS: AR420626, *N*-(2,5-dichlorophenyl)-4-(furan-2-*yl*)-2-methyl-5-oxo-1,4,5,6,7,8-hexahydro-quinoline-3-carboxamide; BiFC, bimolecular fluorescence complementation; CATPB, (*S*)-3-[2-(3-chlorophenyl) acetamido]-4-[4-(trifluoromethyl)phenyl]butanoic acid; CDS, coding regions; CFMB, (2S)-2-(4-chlorophenyl)-3,3-dimethyl-*N*-(5-phenylthiazol-2-yl)butanamide; FBS, fetal bovine serum; FFAR, free fatty acid receptor; FRET, fluorescence resonance energy transfer; HA, hemagglutinin; IHC, immunohistochemistry; NFAT, nuclear factor of activated T cells; PLA, proximity ligation assay; qPCR, quantitative PCR; SCFA, short-chain fatty acid; siRNA, small interfering RNA; TIRF, total internal reflection fluorescence; YFP, yellow fluorescent protein

[1] Correspondence: Department of Biological Science, National University of Singapore, 14 Science Dr. 4, Singapore 117543. E-mail: dbsdjl@nus.edu.sg

This is an Open Access article distributed under the terms of the Creative Commons Attribution-NonCommercial 4.0 International (CC BY-NC 4.0) (http://creativecommons.org/licenses/by-nc/4.0/) which permits noncommercial use, distribution, and reproduction in any medium, provided the original work is properly cited.

doi: 10.1096/fj.201700252RR
This article includes supplemental data. Please visit *http://www.fasebj.org* to obtain this information.

Downloaded from www.fasebj.org by (137.132.3.10) on January 23, 2018. The FASEB Journal Vol. 32, No. 1, pp. 289-303.

mouse colon epithelial cell, both receptors were implicated in the inhibition of p38 and ERK1/2 phosphorylation, leading to reduced colitis (14). In fact, the genetic deletion of either receptor was associated with the colitis phenotype in multiple mouse studies (10–16). In human monocytes, we found that stimulation of either receptor led to elevated p38 phosphorylation (29). The similar phenotypes observed between the aforementioned FFAR2 and FFAR3 studies is consistent with a FFAR2-FFAR3 heteromer-mediated mechanism that was lost upon knockout or knockdown of either receptor subunit.

Here, we show that FFAR2 and FFAR3 do indeed interact to form a GPCR heteromer in monocytes and upon heterologous expression in HEK293 cells. Compared to homomeric FFAR2/3, heteromeric FFAR2-FFAR3 displayed enhanced cytosolic Ca^{2+} signaling and β-arrestin-2 recruitment. Unlike homomeric FFAR2/3, the heteromer lacked the ability to inhibit cAMP production but gained the ability to induce p38 phosphorylation.

MATERIALS AND METHODS

Monocyte isolation and macrophage generation

Monocytes and macrophages were isolated as previously described (29). Human peripheral blood monocytes were isolated from buffy coat of healthy adult donors containing citrate–phosphate–dextrose anticoagulant (National University Hospital, Blood Donation Centre, Singapore). This study was approved by the institutional review board of the National University of Singapore (NUS-IRB B-14-063E). Briefly, the buffy coat was diluted 4 times with PBS containing 2% fetal bovine serum (FBS) and 1 mM EDTA, and the mononuclear fraction was obtained *via* density gradient centrifugation with Ficoll-Paque Premium 1.073 (GE Healthcare, Waukesha, WI, USA). From the mononuclear fraction, the monocyte population was enriched with the Human Monocyte Enrichment Kit (Stemcell Technologies, Vancouver, BC, Canada). Enriched human peripheral blood monocytes were differentiated into macrophages by culture for 7 d in RPMI 1640 medium (with 10% FBS and 1% v/v penicillin and streptomycin) supplemented with 50 ng/ml M-CSF, 37°C, at a cell density of 2×10^6/ml.

Cell culture conditions

Human macrophages and peripheral blood monocytes were cultured in RPMI 1640 medium (with 10% FBS and 1% v/v penicillin and streptomycin) at 37°C for 2 h before being used in assays. HEK293 cells were obtained from the American Type Culture Collection (Manassas, VA, USA) and routinely cultured in DMEM (with 10% FBS and 1% v/v penicillin and streptomycin) at 37°C. Control-HEK293, FFAR2-HEK293, FFAR3-HEK293, and FFAR2-FFAR3-HEK293 cells were cultured in DMEM (with 10% FBS, 1% v/v penicillin and streptomycin, and 2 μg/ml puromycin) at 37°C. HTLA cells were cultured in DMEM (with 10% FBS, 1% v/v penicillin and streptomycin, 2 μg/ml puromycin, and 100 μg/ml hygromycin) at 37°C. All cell lines were routinely tested for mycoplasma contamination.

Generation of HEK293 cells that stably express FFAR2-FFAR3 heteromer

The stop codon was removed from the coding regions (CDS) of human *FFAR3* (NM_005304) and *FFAR2* (NM_005306). These sequences were fused to form a 5′-*FFAR3-E2A-FFAR2*-3′ construct, held together by the *E2A* ribosomal skip sequence (5′-GGAAGCGGACAATGTACTAACTACGCTTTGTTGAAACT-CGCTGGCGATGTTGAAAGTAACCCCGGTCCT-3′). *FFAR2*, *FFAR3*, and *FFAR3-E2A-FFAR2* were cloned in frame into the pCDH-EFI-MCS-T2A-Puro vector (System Biosciences, Palo Alto, CA, USA) to form the pCDH-FFAR2-Puro, pCDH-FFAR3-Puro, and pCDH-FFAR3-FFAR2-Puro expression vectors. These plasmids were transfected into HEK293 cells with the X-tremeGene HP DNA transfection reagent (Roche, Basel, Switzerland) at a final concentration of 1 μg/ml, then selected with 2 μg/ml puromycin (InvivoGen, San Diego, CA, USA) for at least 2 wk to generate the control-HEK293, FFAR2-HEK293, FFAR3-HEK293, and FFAR2-FFAR3-HEK293 cell lines.

Cell treatments

Unless otherwise stated, cells were pretreated for 15 min with either 10 μM YM254890 ($G_{\alpha q}$ inhibitor) or 10 μM (S)-3-[2-(3-chlorophenyl)acetamido]-4-[4-(trifluoromethyl) phenyl]butanoic acid (CATPB; a FFAR2 antagonist) (30, 31) or for 2 h with 500 ng/ml pertussis toxin (Thermo Fisher Scientific, Waltham, MA, USA); and before activation with FFAR2/3 agonists: 10 mM acetate, 10 mM propionate, 10 mM butyrate, and 10 μM (2S)-2-(4-chlorophenyl)-3,3-dimethyl-*N*-(5-phenylthiazol-2-*yl*)butanamide (CFMB; Calbiochem, San Diego, CA, USA) (ChemSpider ID 24656891) (EC_{50} of ~0.7 μM) (32), or 10 μM *N*-(2,5-dichlorophenyl)-4-(furan-2-*yl*)-2-methyl-5-oxo-1,4,5,6,7,8-hexahydro-quinoline-3-carboxamide (AR420626; Glixx Laboratories, Southborough, MA, USA) (EC_{50} of ~0.7 μM) (33).

In situ proximity ligation assays and IHC

Tissue sections were processed and costained for FFAR2 and FFAR3 as previously described (29). Normal human colon sections were obtained from US Biomax (Rockville, MD, USA). HEK293 cells (control-HEK293, FFAR2-HEK293, FFAR3-HEK293, and FFAR2-FFAR3-HEK293), human monocytes, and macrophages were embedded in 1% agarose and fixed overnight with 10% neutral buffered formalin solution followed by embedding with paraffin with tissue processor. After antigen retrieval with 0.01 M citrate buffer pH 6, 20 min at 99°C, tissue sections were stained at 4°C overnight with primary antibodies against FFAR3 (clone 16F4.1; EMD Millipore, Billerica, MA, USA) or FFAR2 (sc-32906; Santa Cruz Biotechnology, Santa Cruz, CA, USA). For the proximity ligation assay (PLA), incubation with the PLA probes (Anti-Rabit Plus, DUO92002, and anti-mouse MINUS, DUO92004; both Sigma-Aldrich, St. Louis, MO, USA) followed by chromogenic substrate development and nuclear staining (Duolink *In Situ* Brightfield Kit, DUO92012; Sigma-Aldrich) was then performed. For immunohistochemical staining, incubation with horseradish peroxidase–polymer anti-mouse IgG (GBI Labs, Mukilteo, WA, USA) was followed by color development with liquid DAB+ substrate (GBI Labs).

Real-time quantitative PCR analysis

Real-time quantitative PCR (qPCR) was performed as previously described (34). RNA was extracted with Trizol reagent (Ambion, Austin, TX, USA). The purified RNA was reverse transcribed with the SuperScript III First-Strand Synthesis system (Thermo Fisher Scientific) and analyzed by real-time qPCR using the GoTaq qPCR Master Mix (Promega, Madison, WI, USA) and a LightCycler 480 (Roche). With *RPL27* (forward: ATCGCCAAGAGATCAAAGATAA; reverse primer: TCTGAAGACATCCTTATTGACG) and *GAPDH*

Downloaded from www.fasebj.org by (137.132.3.10) on January 23, 2018. The FASEB Journal Vol. 32, No. 1, pp. 289-303.

(forward: GAAGGTGAAGGTCGGAGTC; reverse: GGAAGATGGTGATGGGATTTC) as the reference genes, the mean fold change of *FFAR3* (forward: CACCATCTATCTCACCGCCC; reverse: TATGACGTAGACCACGCTGC) and *FFAR2* (forward: GTAGCTAACACAAGTCCAGTCCT; reverse: CTAGGTGTTGCTTTGAAGCTTGT) expression relative to the control-HEK293 cells was calculated using the Relative Expression Software Tool (Rest MCS, v.2) (35, 36).

Bimolecular fluorescence complementation assay

Human *FFAR3* (NM_005304), *FFAR2* (NM_005306), and *P2RY1* (NM_002563), with the start and stop codons deleted, were fused at the 3′ end with a 5′-CGAACCTCCACCTCCACTTCCGCCACCTCCGCTACCACCTCCACC-3′ sequence coding for a GGGGS linker peptide sequence. These constructs were then cloned into either pBiFC-VN155 (I152L) or pBiFC-VC155 plasmids with the N-terminus epitope tags [myc or hemagglutinin (HA), respectively] and C-terminal bimolecular fluorescence complementation (BiFC) fusion partners in frame (37). Twenty nanograms per milliliter of the resulting expression plasmids was transfected into HEK293 cells with the X-tremeGene HP DNA transfection reagent (Roche) with the final concentration topped up to 1 μg/ml with mock plasmid. In coexpression studies, an equimolar ratio of each plasmid was transfected. The Venus fluorescence signals within live cells were imaged *via* inverted fluorescence microscopy (Axio Observer Z1; excitation filter 450–490 nm, emission filter 500–550 nm; Carl Zeiss, Jena, Germany) and quantified *via* flow cytometry (BD LSR Fortessa, 488-nm solid laser, 530/30-nm emission filter; BD Biosciences, San Jose, CA, USA). For the flow cytometry measurement of myc and HA epitope tag expression levels, transfected HEK293 cells were detached with PBS containing 2% FBS and 1 mM EDTA, and fixed for 10 min with 2% paraformaldehyde at room temperature. The cells were then blocked for 20 min at 4°C in blocking buffer (PBS containing 2% FBS, 1 mM EDTA, and 0.5% Tween 20) before staining for myc with 5 μg/ml mouse anti-human c-myc p67 (clone 9E10; eBioscience, San Diego, CA, USA) or for HA using 10 μg/ml HA tag mAb (clone 2-2.2.14; Thermo Fisher Scientific), at 4°C for 20 min. This was followed by secondary antibody staining using donkey anti-mouse IgG, Alexa Fluor 488 (Thermo Fisher Scientific), at 4°C for 20 min. The stained cells were analyzed *via* flow cytometry (BD LSR Fortessa, 488-nm solid laser, 530/30-nm emission filter). Flow cytometry data were expressed as the median fluorescence intensity of 20,000 cells (mean ± SD, $n = 3$).

Live-cell fluorescence resonance energy transfer and calcium imaging

Live-cell imaging for GCAMP3 and yellow fluorescent protein (YFP) was recorded using a Nikon Ti inverted microscope (Nikon, Tokyo, Japan) with 491-nm laser under the total internal reflection fluorescence (TIRF) imaging mode (iLAS2 of Roper Scientific, Tucson, AZ, USA) to reduce phototoxicity. The 561-nm laser was used for mCherry. All images were acquired through Nikon objectives (Apo TIRF ×60, N.A. 1.49 oil) and a quad-bandpass filter (Di01-R405/488/561/635; Semrock, Rochester, NY, USA) and by a Prime 95B CMOS camera (Photometrics, Tucson, AZ, USA). GCAMP3, YFP, and mCherry fluorescence was acquired through 525/45-, 525/45-, and 609/54-nm emission filters, respectively. The microscope was controlled by MetaMorph 7.8 software (Universal Imaging, Bedford Hills, NY, USA). Postacquisition image analysis was performed using Fiji (*https://fiji.sc/*) and MatLab (MathWorks, Natick, MA, USA). During imaging, the cells were maintained in 2 ml medium [FluoroBrite DMEM (Thermo Fisher Scientific), 10% FBS, and 1% v/v penicillin and streptomycin] and placed in a live imaging incubator stage set at 37°C and perfused with 5% CO_2.

For the acceptor photobleaching fluorescence resonance energy transfer (FRET) experiments, FFAR2 and FFAR3 with C-terminal YFP tags were expressed from pcDNA5/FRT/TO expression plasmids. These plasmids were the kind gift of G. Milligan (University of Glasgow, Glasgow, United Kingdom) (38). GLUT4mCherry was generated by inserting the GLUT4 CDS (without stop codon) into the pmCherry-N1 vector at the *Eco*RI and *Bam*HI restriction sites. HEK293 cells were plated in 35-mm glass-bottom culture dishes (MatTek, Ashland, MA, USA). One day before imaging, these cells were transfected with an equimolar ratio of the YFP- and mCherry-tagged receptor plasmids with the X-tremeGene HP DNA transfection reagent (Roche) at a final combined concentration of 1 μg/ml. Live cell imaging was performed with a 2-s interval between image captures. In between two images captured, mCherry photobleaching was achieved by exposing a 60- × 60-pixel area to the 561-nm laser for 60 passes. Upon background subtraction, the images captured immediately before and after photobleaching were used to calculate the percentage change in YFP fluorescence, which is defined as the difference in the fluorescence intensity (measured in a 30- × 30-pixel region of interest) between the after and before images, divided by the intensity of the before image. Representatives of these images were used to generate the pseudocolor (Fiji) and monochromatic images.

For the live-cell calcium imaging assays, control-HEK293, FFAR2-HEK293, FFAR3-HEK293, and FFAR2-FFAR3-HEK293 cells were plated in 35-mm glass-bottom culture dishes (MatTek). One day before imaging, the cells were transfected with 1 μg/ml GCaMP3 plasmid (39) using X-tremeGene HP DNA transfection reagent (Roche). During live imaging, stimulations were performed by adding 2 ml 20 mM acetate in the medium to achieve a final concentration of 10 mM acetate. Pseudocolor images were generated using the Thermal lookup table in Fiji. The mean fluorescence intensity of an arbitrarily chosen region of interest on the cells (15 × 15 pixels) (F) was divided with the mean intensity in the same region before stimulation (F_0) to obtain the peak amplitude of the GCaMP3 signal (F/F_0). The fluorescence half-time is defined as the time interval starting when the fluorescence signal is at half maximal intensity before the fluorescence peak, and ending when the fluorescence signal is again at half maximal intensity after the same fluorescence peak.

cAMP GloMax and nuclear factor of activated T cells reporter assays

The cAMP GloMax assay (Promega) was used to measure cAMP inhibition in control-HEK293, FFAR2-HEK293, FFAR3-HEK293, and FFAR2-FFAR3-HEK293 cells. The protocol used here was adapted from Promega (40). Briefly, cells were suspended in induction buffer (PBS with 1 mM 3-isobutyl-1-methylxanthine, 0.2 mM Ro20, and 12.5 mM $MgCl_2$) at 250 cells/μl and seeded into 96-well plates at 20 μl/well. Ten microliters of induction buffer with 4 times the required concentration of ligand (40 mM acetate or propionate) was added, followed by a 10-min incubation. This was followed by the addition of 10 μl induction buffer containing 20 μM forskolin with a 15-min incubation (at this stage, the cells were in 10 mM acetate/propionate and 5 μM forskolin in a final volume of 40 μl). Next, 10 μl cAMP detection solution was added before incubation for 20 min with shaking. Finally, 50 μl Kinase Glo reagent was added, and the sample was incubated for 10 min before the luminescence signal was measured with a GloMax 20/20 luminometer (Promega). A nuclear factor of activated T cells (NFAT) luciferase reporter

Downloaded from www.fasebj.org by (137.132.3.10) on January 23, 2018. The FASEB Journal Vol. 32, No. 1, pp. 289-303.

assay was used to measure Ca^{2+} signaling in control-HEK293, FFAR2-HEK293, FFAR3-HEK293, and FFAR2-FFAR3-HEK293 cells. Briefly, the cells were transfected with 1 μg/ml NFAT luciferase reporter plasmid using X-tremeGene HP DNA transfection reagent (Roche) and incubated overnight. The cells were split into 96-well plates, induced overnight with SCFAs, and the luciferase signals measured with the Promega Luciferase Assay system using GloMax 20/20 luminometer.

Tango β-arrestin-2 recruitment assays

Recruitment rates for β-arrestin-2 were measured using the Tango assay (41), whereby FFAR2 or FFAR3 constructs with C-terminal tTa transcription factor fusions (FFAR2/3tTa) were expressed from FFA2-Tango, FFA3-Tango, and P2RY1-Tango plasmids (plasmids 66281, 66282, and 66468; Addgene, Cambridge, MA, USA) in HTLA cells. HTLA are HEK293 cells containing a tTa-dependent firefly luciferase reporter gene and expressing β-arrestin-2 fused with tobacco etch virus (TEV) protease (41, 42). Binding of β-arrestin-2-TEV to FFAR2/3tTa would lead to cleavage of the tTa transcription factor that would then drive luciferase reporter expression. The CDS of human *FFAR3* (NM_005304) and human *FFAR2* (NM_005306) were cloned into the pcDNA3.1/V5-His A (Thermo Fisher Scientific) expression vector as described in our previous study (29). The HTLA cells were transfected with 1 μg/ml expression plasmids using X-tremeGene HP DNA transfection reagent (Roche) and incubated overnight. An equimolar ratio of 2 plasmid types was transfected: a FFA2/FFA3/P2RY1-Tango plasmid with a pcDNA3.1/V5-His A expression vector with no insert for single-expression studies, or a FFA2/FFA3/P2RY1-Tango plasmid with a pcDNA3.1/V5-His A expression vector with the FFAR2 or FFAR3 CDS inserted for coexpression studies. Then the cells were split into 96-well plates. After overnight induction with agonists, the luciferase signals were measured with the Promega Luciferase Assay system and the GloMax 20/20 luminometer.

Western blot analysis of p38 and ERK1/2

HEK293 cells were cultured in 24-well plates till near confluence. Subsequently, the cell culture medium was replaced with serum-free DMEM for overnight culture before agonist stimulations. Total cell lysates were resolved on a denaturing SDS-PAGE gel (10%) and transferred onto PVDF membranes *via* the Trans-Blot Turbo Transfer system (Bio-Rad, Hercules, CA, USA). These were then probed with antibodies against phospho-p38 (Thr180/Tyr182) (4511; Cell Signaling Technology, Danvers, MA, USA), p38 (8690; Cell Signaling Technology), phospho-ERK1/2 (Thr202/Tyr204) (4370; Cell Signaling Technology), or ERK1/2 (9107; Cell Signaling Technology). These primary antibodies were then probed with the respective horseradish peroxidase–conjugated secondary antibodies. Western blot chemiluminescent signals were captured with an ImageQuant LAS 4000 mini imager (GE Healthcare). Densitometric analysis was performed on biologic triplicates using ImageQuant TL software (GE Healthcare). These PVDF blots were then stripped with Restore Western blot stripping buffer (Thermo Fisher Scientific) before reprobing.

Statistical analysis

Differences between averages were analyzed by the 2-tailed Welch's unequal variance *t* test. Significance was set at $P < 0.05$, $P < 0.01$, and $P < 0.001$.

RESULTS

FFAR2-FFAR3 heteromerize in primary monocytes and macrophages

The formation of FFAR2-FFAR3 heteromers in primary tissues would suggest a role for the heteromer in physiologic processes. Human colon epithelial cells, monocytes, and macrophages were previously found to coexpress FFAR2 and FFAR3 (27–29), making these cells potential targets for the detection of FFAR2-FFAR3 heteromerization. Heteromerization was probed *via in situ* PLA (**Fig. 1**), which produced red and brown spots upon positive interaction. PLA detected FFAR2-FFAR3 heteromerization in human monocytes and macrophages, but not in colon epithelial cells. Because all 3 cell types stained positive for FFAR2 and FFAR3 in our previous study *via* IHC (29), this suggests that the coexpression of FFAR2 and FFAR3 alone, as was observed in colon epithelial cells, does not necessarily lead to FFAR2-FFAR3 heteromer formation. Cell-specific heteromerization has been observed for other GPCRs such as the D_1-D_2 dopamine heteromer (43). The cell-specific PLA staining is also consistent with a specific PLA signal that was only generated upon heteromer formation. These PLA assays putatively confirm that endogenous FFAR2-FFAR3 heteromers exist in primary tissues such as monocytes and macrophages, prompting further investigation.

FFAR2-FFAR3 homomers and FFAR2-FFAR3 heteromers are formed in HEK293

To further explore the interaction between FFAR2 and FFAR3, we performed acceptor photobleaching FRET assays (44). FFAR2, FFAR3, and GLUT4 were tagged at the C terminus with either YFP or mCherry. YFP-tagged receptors were then transiently coexpressed with mCherry-tagged receptors in HEK293, where presumably the interaction between the coexpressed receptors would lead to FRET. Since a portion of the YFP (donor) emission is transferred to mCherry (acceptor) during FRET, the photobleaching of mCherry would lead to a recovery or increase in direct YFP fluorescence. This was observed for both the FFAR2YFP-FFAR2mCherry and FFAR3YFP-FFAR2mCherry pairings (8.5 ± 4.6 and 10.2 ± 3.6%, respectively) (**Fig. 2*A*, *B***). The FFAR2YFP-FFAR2mCherry pairing acted as a positive control as the homomerization of FFAR2 has been observed in HEK293T cells *via* time resolved FRET and coimmunoprecipitation assays (45). On the other hand, no such recovery in direct YFP fluorescence upon mCherry photobleaching was observed for the non-interacting negative control pair of FFAR3YFP-GLUT4mCherry. Thus, our FRET assays suggest that FFAR2-FFAR3 heteromerization occurs in HEK293 cells.

The FFAR2-FFAR3 interaction was also detected by BiFC assays. Here, FFAR2, FFAR3, and P2Y purinoceptor 1 (P2RY1) were tagged at the C terminus with the VN or VC pBiFC fragments, respectively. These receptor fusion constructs were transiently expressed in HEK293 cells, with comparable levels of expression between constructs (Fig. 2*C*). Unlike the FRET assays, which required

Downloaded from www.fasebj.org by (137.132.3.10) on January 23, 2018. The FASEB Journal Vol. 32, No. 1, pp. 289-303.

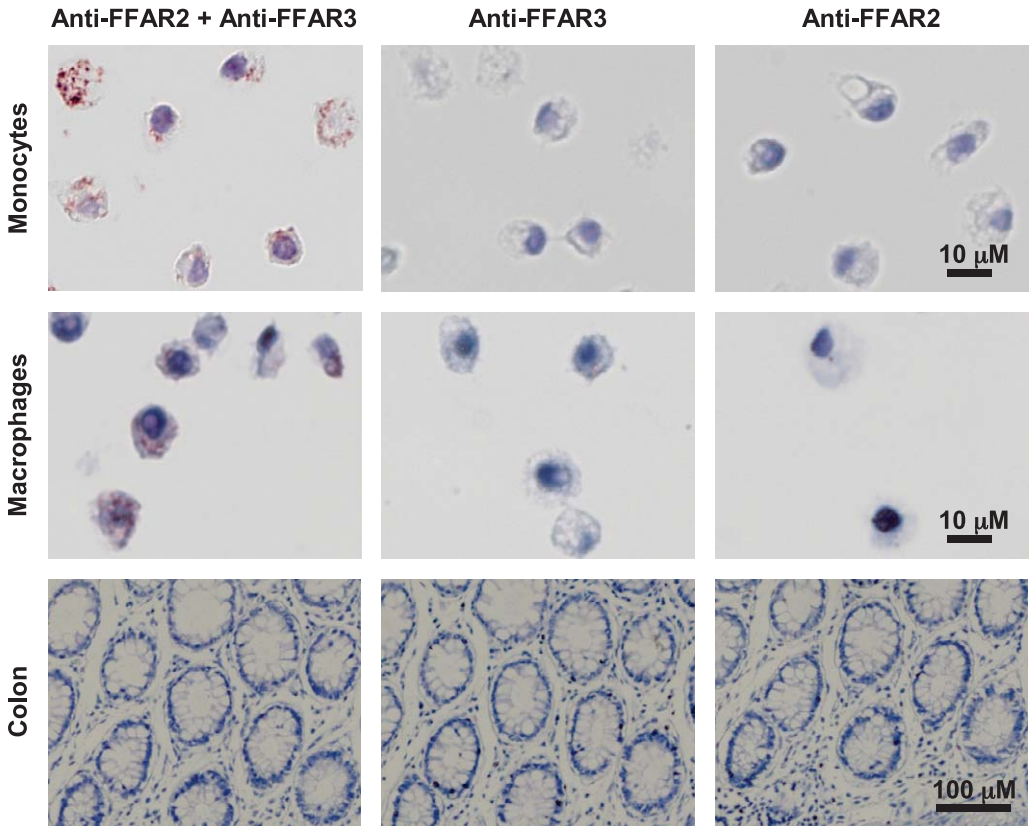

Figure 1. FFAR2-FFAR3 heteromer is expressed in human monocytes and macrophages. *In situ* PLA of human paraffin-embedded tissue sections of peripheral blood monocytes, macrophages, and colon epithelial cells. Red and brown spots indicate positive PLA signals when anti-FFAR2 and anti-FFAR3 PLA probe pairs are in proximity. Samples probed without one of the primary antibodies act as negative controls. All samples were probed in parallel. Data shown are representative of 3 independent experiments.

overexpression of the fluorescent protein–tagged receptors to generate a detectable FRET signal, the BiFC experiments were performed at reduced receptor expression levels by lowering the concentration of expression plasmids used during transfection (20 ng/ml of each VN and VC expression plasmid) (Supplemental Fig. 1). This reduced the likelihood of artifacts from overexpression. The formation of receptor oligomers was then investigated through the coexpression of receptor constructs, where presumably oligomerization would allow for the complementary VN and VC fragments to reform the functional Venus fluorescent protein and generate a fluorescence signal. FFAR3 homomerization and FFAR2-FFAR3 heteromerization was detected, as the FFAR3VN-FFAR3VC, FFAR2VN-FFAR3VC, and FFAR2VC-FFAR3VN pairings were significantly more fluorescent than the negative control pairings of FFAR2/3+P2RY1 (30% or less) (Fig. 2*D, E*). P2RY1 was selected as a negative control for FFAR2 and FFAR3 because phylogenetic analyses have classified all 3 receptors as part of the same subfamily A11 of rhodopsin-like GPCRs (46). *Via* FRET analysis, P2RY1 had been reported to display partial levels of homomerization (44%) and is only fully homomeric (85–100%) upon agonist exposure (47). This lack of agonist induction may account for the lack of significant fluorescence intensity difference between the P2YR1VN-P2YR1VC pairing and the brightest negative control pair of P2RY1VN + FFAR3VC. Significantly, the fluorescence signal intensities of the FFAR3VN-FFAR3VC, FFAR2VN-FFAR3VC, and FFAR2VC-FFAR3VN pairings were comparable to homomeric FFAR2VN-FFAR2VC positive control (Fig. 2*D, E*), which suggests that the FFAR3 homomer and FFAR2-FFAR3 heteromer are formed at nearly the same frequency as the known FFAR2 homomer (44).

As GPCRs, FFAR2/3 are expected to localize on the cell surface, which we observed (Fig. 2*C*). Interestingly, a fraction of the FFAR2/3 oligomers appeared to localize intracellularly, and persisted even at reduced FFAR2 expression levels (which was achieved by reducing plasmid concentration during transfection) (Supplementa1 Fig. 1). We note that this partial intracellular localization was also displayed during transient expression of cyan fluorescent protein– and YFP-tagged FFAR2/3 in HEK293T [see figs. 5.9, 5.12, and 6.3 of Stoddart *et al.* (44)]. The intracellular FFAR2/3 fraction may be due to constitutive internalization of agonist-free GPCR, which has been observed for a subset of GPCRs, such as the putative nutrient sensing receptor GPRC6A (48) and the atypical chemokine receptor 3 (49). Confirming this will require further studies. Conversely, the control P2RY1 receptor, which was previously found to internalize only upon agonist induction (47), displayed mostly cell surface localization (Fig. 2*C*) despite being expressed at levels comparable to FFAR2/3 (Fig. 2*A*). Cumulatively, our BiFC

Downloaded from www.fasebj.org by (137.132.3.10) on January 23, 2018. The FASEB Journal Vol. 32, No. 1, pp. 289-303.

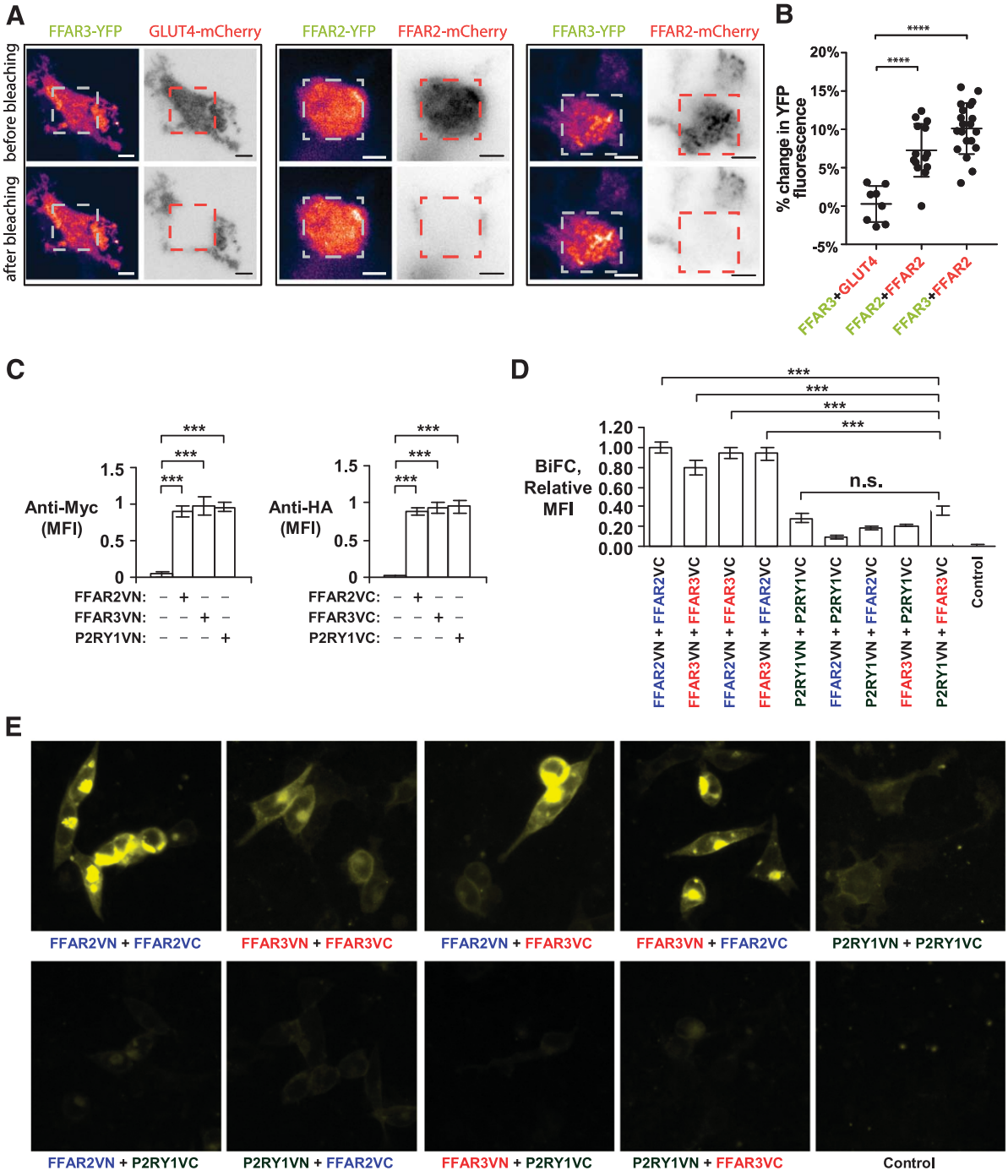

Figure 2. BiFC and FRET assays detect heteromer and homomer formation during coexpression of FFAR2 and FFAR3 in HEK293 cells. *A*, *B*) YFP-tagged FFAR2/FFAR3 were coexpressed with mCherry-tagged FFAR2/GLUT4 in HEK293 cells. *A*) Representative TIRF microscopy images are shown, with fluorescence intensity detected by YFP and mCherry channels displayed in pseudocolor and monochrome, respectively. Images were captured before and after photobleaching of mCherry in a 60- × 60-pixel region of interest, as denoted by red dashed squares, with before and after images captured 2 s apart. Scale bars, 5 μm. *B*) These before and after photobleaching images (YFP channel) were used to calculate percentage change in YFP fluorescence. For FFAR3YFP-GLUT4mCherry, $n = 8$ cells were from 2 experiments; for FFAR2YFP-FFAR2mCherry, $n = 15$ cells were from 3 experiments; for FFAR3YFP-FFAR2mCherry, $n = 22$ cells were from 3 experiments. Error bar indicates SD. $^{****}P < 0.0001$, Student's t test. *C–E*) FFAR2, FFAR3, and P2RY1 were tagged at N terminus with myc or HA epitopes, and at C terminus with VN or VC pBiFC fragments, respectively. These constructs were transiently expressed in HEK293, and their expression levels were determined *via* immunostaining of myc/HA tags followed by flow cytometry analysis (*C*). Upon coexpression of these constructs, interaction of receptors would allow for VN and VC fragments to reconstitute full Venus fluorescent protein. Resulting gain in fluorescence signal was measured in live cells *via* flow cytometry (*D*) and fluorescence microscopy (*E*). Flow cytometry readings are expressed as median fluorescence intensity (MFI) of 20,000 cells. Values shown are means ± SD of triplicate transfections. FFAR2VN-FFAR2VC sample has been arbitrarily assigned value of 1. Two-tailed Welch's t test was used to determine statistical significance. $P < 0.05$, $^{**}P < 0.01$, $^{***}P < 0.001$.

Downloaded from www.fasebj.org by (137.132.3.10) on January 23, 2018. The FASEB Journal Vol. 32, No. 1, pp. 289-303.

and FRET assays further corroborate FFAR2-FFAR3 heteromerization, in addition to detecting homomeric FFAR3.

Stable expression of FFAR2-FFAR3 in HEK293 cells as a model to investigate heteromer signaling

The discovery of the FFAR2-FFAR3 heteromer opens up the possibility of investigating the role of heteromerization in physiologic processes. FFAR2/3-knockout animals are ill suited for such a purpose because they are likely to lose both homomer- and heteromer-dependent functions. Fortunately, the formation of the FFAR2-FFAR3 heteromer upon the coexpression of FFAR2 and FFAR3 in HEK293 cells (Fig. 2) allowed us to generate HEK293 cells that stably expressed the FFAR2-FFAR3 heteromer *via* coexpression of both receptor subunits (FFAR2-FFAR3-HEK293), as well as control cells with stable single-expression of homomeric FFAR2 (FFAR2-HEK293) and FFAR3 (FFAR3-HEK293). To closely replicate endogenous receptor function, only wild-type untagged FFAR2 and FFAR3 were expressed. Real-time qPCR and IHC detected comparable FFAR2 expression between FFAR2-HEK293 and FFAR2-FFAR3-HEK293, whereas FFAR3 expression was comparable between FFAR3-HEK293 and FFAR2-FFAR3-HEK293 (Supplemental Fig. 2). We then examined whether signaling from heteromeric FFAR2-FFAR3-HEK293 is distinct from homomeric FFAR2-HEK293 and FFAR3-HEK293. This is a novel approach because previous studies on the signaling of FFAR2 ($G_{\alpha i}$ and $G_{\alpha q}$ coupled) and FFAR3 ($G_{\alpha i}$ coupled) were performed with single receptor expression systems, where presumably only signaling from the homomers was evaluated (1, 2).

FFAR2-FFAR3 heteromerization elevates Ca^{2+} signaling

First we examined the effect of FFAR2-FFAR3 heteromer formation on the Ca^{2+} signaling pathway, which is elevated by FFAR2 *via* $G_{\alpha q}$ coupling (1, 2). FFAR2-induced Ca^{2+} signaling has been associated with obesity (8). Hence, the modulation of this pathway by the FFAR2-FFAR3 heteromer may have important physiologic implications. To capture the high Ca^{2+} binding affinities and fast kinetics in live cells, intracellular Ca^{2+} changes were monitored with the Ca^{2+} indicator GCaMP3 (39). Upon stimulation with 10 mM acetate, we observed an immediate increase in cytosolic Ca^{2+} concentration in FFAR2-HEK293 and FFAR2-FFAR3-HEK293, while no significant changes were detected in FFAR3-HEK293 and control-HEK293 (**Fig. 3*A*, *B***). Notably, the amplitude of the acetate-induced Ca^{2+} signal was higher in FFAR2-FFAR3-HEK293 ($F/F_0 = 4.0 \pm 0.3$, $n = 31$ cells) relative to that of FFAR2-HEK293 ($F/F_0 = 2.5 \pm 0.4$, $n = 33$ cells) (Fig. 3*A*–*C*). This elevated Ca^{2+} signal also lasted significantly longer in FFAR2-FFAR3-HEK293 cells (half-time, 186.0 ± 21.7 s, $n = 28$ cells) than in FFAR2-HEK293 (half-time, 108.5 ± 16.5 s, $n = 32$ cells) (Fig. 3*D*). The enhancement in Ca^{2+} signaling was corroborated by another reporter system, the NFAT reporter (Fig. 3*E*). Consistent with imaging assays, acetate/propionate-induced NFAT reporter activity was enhanced in FFAR2-FFAR3-HEK293 (1.5-fold increase over FFAR2-HEK293). In both FFAR2-HEK293 and FFAR2-FFAR3-HEK293, the induction of the NFAT reporter by acetate/propionate was abolished upon treatment with either FFAR2 antagonists or the $G_{\alpha q}$ pathway inhibitor (YM254890), consistent with a FFAR2- and $G_{\alpha q}$-dependent mechanism. Overall, both the GCaMP3 and NFAT reporters reveal a role for FFAR2-FFAR3 heteromerization in elevating Ca^{2+} signaling.

Ability to inhibit cAMP production is lost upon FFAR2-FFAR3 heteromerization

We then examined whether heteromerization alters the ability of FFAR2 and FFAR3 to inhibit cAMP production *via* $G_{\alpha i}$ coupling (1, 2), which are important pathways implicated in diabetes (3). Cellular cAMP levels were assayed *via* the cAMP GloMax reporter, which produced a luminescence signal that was inversely proportional to the concentration of cAMP (Fig. 3*F*). Upon acetate or propionate treatment, the production of forskolin-induced cAMP was inhibited in both FFAR2-HEK293 and FFAR3-HEK293, but not FFAR2-FFAR3-HEK293 and control-HEK293 cells. This suggests that the ability of the FFAR2/3 subunits to inhibit cAMP production may be lost upon heteromerization. The inhibition of cAMP observed during acetate and propionate treatment was blocked in FFAR2-HEK293 but not FFAR3-HEK293 during FFAR2 antagonism, consistent with a receptor-specific effect. The inhibitory activity was also blocked in both FFAR2-HEK293 and FFAR3-HEK293 by pertussis toxin ($G_{\alpha i}$ inhibitor) treatment, consistent with the expected $G_{\alpha i}$-protein-coupled mechanism of these receptors (1, 2).

FFAR2-FFAR3 heteromerization markedly enhanced the recruitment of β-arrestin-2

Besides G-protein-coupling, β-arrestin-2 recruitment has also been observed for FFAR2 (50, 51). Here, we investigated the effect of FFAR2-FFAR3 heteromerization on β-arrestin-2 recruitment. Using the Tango assay (42), a reporter luciferase signal is generated proportional to β-arrestin-2 binding to FFAR2/3Ta [FFAR2/3 with C-terminal tTa fusions (41)]. Ligand (acetate, propionate, butyrate, or FFAR2 agonist) treatment induced β-arrestin-2 recruitment to homomeric FFAR2tTa and heteromeric FFAR2tTa-FFAR3 at comparable levels (**Fig. 4*A*, *B***). Interestingly, β-arrestin-2 recruitment was also detected for homomeric FFAR3tTa upon ligand (propionate, butyrate, and FFAR3 agonist) treatment, and the recruitment rate was 10- to 30-fold higher for heteromeric FFAR2-FFAR3tTa. The enhancement in β-arrestin-2 recruitment to heteromeric FFAR2-FFAR3tTa was particularly pronounced during acetate treatment (Fig. 4*A*), where β-arrestin-2 recruitment was only observed for FFAR2-FFAR3tTa heteromer, while FFAR3tTa homomer remained unresponsive. This enhancement was observed even during treatment with the FFAR3-specific agonist

Downloaded from www.fasebj.org by (137.132.3.10) on January 23, 2018. The FASEB Journal Vol. 32, No. 1, pp. 289-303.

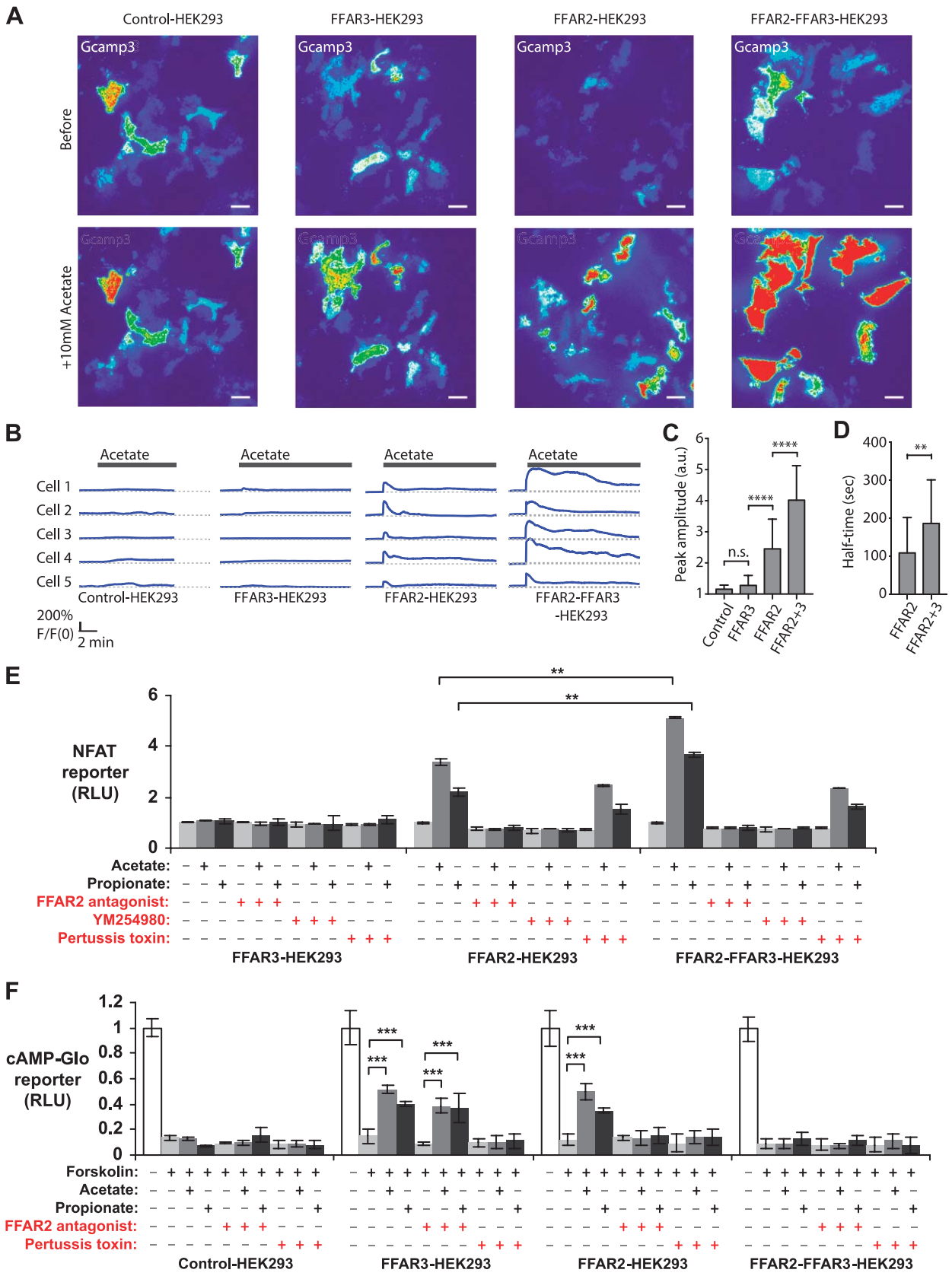

Figure 3. FFAR2-FFAR3 heteromerization enhances Ca^{2+} signaling *via* pertussis toxin–sensitive mechanism while attenuating cAMP inhibition. Assays were performed on HEK293 cells that stably express FFAR3, FFAR2, or both (control-, FFAR3-, FFAR2- and FFAR2-FFAR3-HEK293). *A–D*) Cytosolic Ca^{2+} levels upon 10 mM acetate stimulation as measured *via* GCaMP3 Ca^{2+} reporter. Reporter fluorescence is proportional to Ca^{2+} concentration and was quantified *via* TIRF microscopy. *A*) GCaMP3 fluorescence represented with pseudocolor lookup table before and during peak response after acetate stimulation. *B*) Representative time

(*continued on next page*)

Downloaded from www.fasebj.org by (137.132.3.10) on January 23, 2018. The FASEB Journal Vol. 32, No. 1, pp. 289-303.

AR420626 (Fig. 4*B*) (33). AR420626 is unlikely to have significantly activated the FFAR2 subunit because the same treatment failed to induce β-arrestin-2 recruitment to homomeric FFAR2tTa (Fig. 4*D*). During coexpression of the negative control noninteracting pairs of P2RY1tTa + FFAR2 (Fig. 2), the rate of β-arrestin-2 recruitment upon P2RY1 ligand (ATP) induction was instead partially reduced relative to single expression of P2RY1tTa alone, perhaps due to competition for β-arrestin-2 during coexpression (Fig. 4*C*). This suggests that the β-arrestin-2 recruitment enhancement is dependent on the formation of the FFAR2-FFAR3 heteromer. The marked increase in β-arrestin-2 recruitment upon FFAR2-FFAR3 heteromerization described here suggests that β-arrestin-2 signaling may play a larger role than what was previously anticipated in FFAR2/3 function. This is a possibility that warrants further study.

FFAR2-FFAR3 heteromerization enables p38 phosphorylation in HEK293 cells and possibly monocytes

FFAR2 and FFAR3 have been implicated in the induction of p38 phosphorylation by SCFAs in mouse neutrophils (11, 52) and colon epithelial cells (14) during colitis as well as in our own study in human monocytes during inflammatory responses (29). Here, we found that FFAR2-FFAR3 heteromerization may mediate the phosphorylation of p38 observed. This is based on the finding that only the FFAR2-FFAR3 heteromer (in FFAR2-FFAR3-HEK293) displayed the ability to induce p38 phosphorylation during acetate or propionate treatment—an ability that was otherwise not observed in homomeric FFAR2 and FFAR3 cells (FFAR2-HEK293 and FFAR3-HEK293) (**Fig. 5*A***). FFAR2 and FFAR3 have also been implicated in ERK1/2 phosphorylation, which was observed upon acetate stimulation of HEK293 cells expressing YFP-tagged FFAR2 or FFAR3 (38). Here, we observed the same effect in FFAR2-HEK293 and FFAR3-HEK293 cells, as well as in FFAR2-FFAR3-HEK293 (Fig. 5*A*).

FFAR2-FFAR3 heteromer-mediated signaling in HEK293 cells and monocytes is sensitive to FFAR2 antagonism, $G_{\alpha q}$ inhibition, and $G_{\alpha i}$ inhibition

In HEK293 cells that expressed the FFAR2-FFAR3 heteromer (FFAR-FFAR3-HEK293 or FFAR3tTa-FFAR2-HEK293), the antagonism of FFAR2 (*via* CATPB (30, 31)) attenuated agonist-induced Ca^{2+} signaling (Fig. 3*E*), β-arrestin-2 binding (Fig. 4*D*), and the phosphorylation of p38 and ERK1/2 (Fig. 5*A*). The inhibitory activity of CATPB was specific for FFAR2 because the same treatment did not inhibit the induction of these pathways in cells expressing homomeric FFAR3 alone (FFAR3-HEK293 or FFAR2-tTa-HEK293). Further downstream, $G_{\alpha q}$ inhibition *via* YM254890 (53) almost completely abolished β-arrestin-2 recruitment (Fig. 4*D*) and p38 phosphorylation of the FFAR2-FFAR3 heteromer (Fig. 5*B*). This is consistent with the observation that the FFAR2-FFAR3 heteromer elevates intracellular Ca^{2+} *via* YM254890-sensitive $G_{\alpha q}$ coupling (Fig. 3*E*). As a negative control, YM254890 had no effect on β-arrestin-2 recruitment to homomeric FFAR3-tTa (Fig. 4*D*), which was not observed to induce Ca^{2+} (Fig. 3*E*). Interestingly, pertussis toxin ($G_{\alpha i}$ inhibitor) treatment abolished the enhancement in Ca^{2+} signaling to heteromeric FFAR2-FFAR3-HEK293 (Fig. 2*E*) and β-arrestin-2 recruitment to heteromeric FFAR3tTa-FFAR2 (Fig. 4*D*). The resulting reporter activities were comparable to that of homomeric FFAR2-HEK293 and FFAR3tTa, respectively. This suggests that $G_{\alpha i}$ activity is required for the enhancement. The pertussis toxin treatment used was effective at inhibiting $G_{\alpha i}$ activity, as the same treatment abolished the inhibition of cAMP production observed in FFAR2-HEK293 and FFAR3-HEK293 (Fig. 3*F*).

Acetate-induced p38 phosphorylation in monocytes was abolished by $G_{\alpha q}$ inhibition (29) and by FFAR2 antagonism (Fig. 5*C*) but not pertussis toxin treatment (29). The same inhibitor sensitivity pattern was observed for the induction of p38 in FFAR2-FFAR3-HEK293 cells (Fig. 5*A, B*). This suggests that like FFAR2-FFAR3-HEK293 cells, p38 phosphorylation in monocytes is mediated by the FFAR2-FFAR3 heteromer. Hence, our results suggest that signaling from the FFAR2-FFAR3 heteromer is susceptible to FFAR2 antagonism, $G_{\alpha q}$ inhibition, and $G_{\alpha i}$ inhibition.

DISCUSSION

FFAR2-FFAR3 heteromer may be involved in a number of FFAR2/3-associated diseases

Here, we reveal that FFAR2 and FFAR3 interact to form a heteromer with downstream signaling that is distinct from the parent homomers (**Fig. 6**). Future studies will need to account for the possibility that the disease phenotypes (*e.g.*, obesity, colitis, colon cancer, asthma, and arthritis) observed in mice upon the single knockout of either FFAR2 or FFAR3 (3–20) may be due to the concomitant loss of the

series of GCaMP3 fluorescence intensity upon acetate stimulation. *C, D*) Quantification of GCaMP3 fluorescence peak amplitude (F/F_0) (*C*) and fluorescence half-times (*D*). *F*, fluorescence intensity after stimulation. F_0, intensity before stimulation. For control-HEK293, $n = 21$ cells from 2 experiments; for FFAR3-HEK293, $n = 30$ cells from 2 experiments; for FFAR2-HEK293, $n = 33$ cells from 3 experiments, and for FFAR2-FFAR3-HEK293, $n = 31$ cells from 3 experiments. A.u., arbitrary units; n.s., nonsignificant. Scale bars for fluorescence images, 10 μm; for time-series profiles, 2 min (horizontal). *E*) NFAT luciferase reporter assay activity upon overnight induction with 10 mM acetate or 10 mM propionate. Reporter activity is proportional to Ca^{2+} concentration. Values shown are averages ± SD of triplicate treatment groups ($n = 3$). All values have been standardized to untreated control, which was arbitrarily set to 1. *F*) Effect of acetate/propionate treatments on induction of cAMP by 5 μM forskolin. Luminescence signal from cAMP GloMax kit (Promega) is inversely proportional to cAMP concentration. Values shown are averages ± SD of replicate treatment groups ($n = 5$). All values are relative to untreated control, which was set to 1. Two-tailed Welch's *t* test was used to determine statistical significance. $*P < 0.05$, $**P < 0.01$, $***P < 0.001$, $****P < 0.0001$.

Downloaded from www.fasebj.org by (137.132.3.10) on January 23, 2018. The FASEB Journal Vol. 32, No. 1, pp. 289-303.

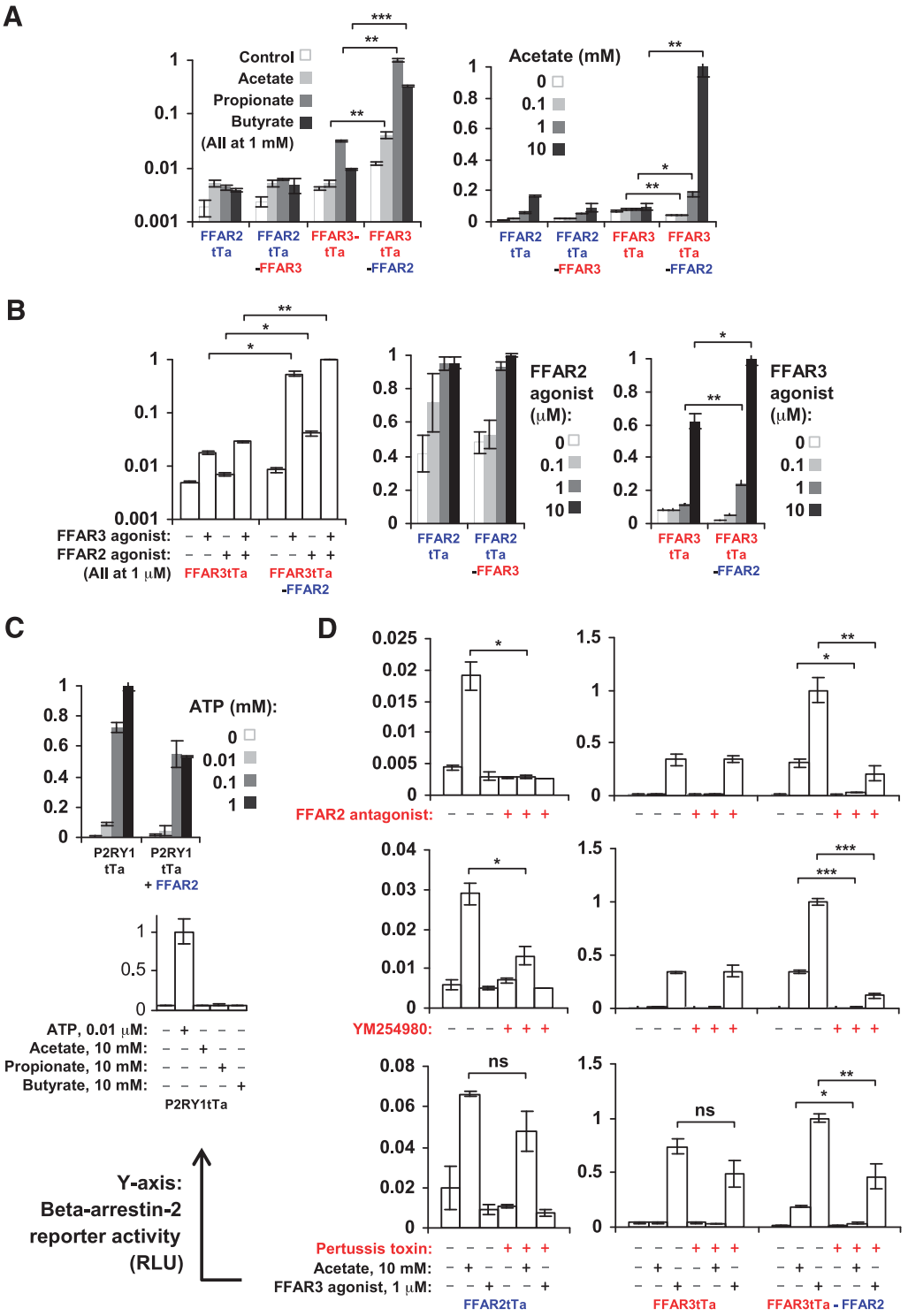

Figure 4. FFAR2-FFAR3 heteromerization enhances β-arrestin-2 recruitment to FFAR3 subunit *via* mechanism sensitive to FFAR2 antagonism, $G_{\alpha i}$ inhibition, and pertussis toxin. β-Arrestin-2 recruitment rates to FFAR2/3tTa (FFAR2/3 receptors with C-terminal tTa fusions) upon overnight induction with acetate, propionate, butyrate, and FFAR2/3 agonist. Reporter activity is proportional to β-arrestin-2 recruitment rates. Cells expressed either homomeric FFAR2tTa, homomeric FFAR3tTa, heteromeric FFAR2tTa-FFAR3, or heteromeric FFAR3tTa-FFAR2. *A*) β-Arrestin-2 reporter activity during SCFA agonist (acetate, propionate, and butyrate) stimulation. *B*) β-arrestin-2 reporter activity during receptor specific agonist stimulation. *C*) β-Arrestin-2 reporter activity during coexpression of FFAR2 with noninteracting receptor P2YR1tTa upon overnight induction with ATP at indicated concentration. *D*) β-Arrestin-2 recruitment during FFAR2 antagonism (CATPB), $G_{\alpha q}$ inhibition (YM254890), and $G_{\alpha i}$ inhibition (pertussis toxin). Data shown are means of triplicate treatment groups ($n = 3$) ± SD and are representative of 3 independent experiments. Highest reading has been arbitrarily assigned value of 1. Two-tailed Welch's *t* test was used to determine statistical significance. $^*P < 0.05$, $^{**}P < 0.01$, $^{***}P < 0.001$.

heteromer and its unique signaling output. In fact, the association of both FFAR2- and FFAR3-knockout mice with the same colitis phenotype (10–16) is consistent with a FFAR2-FFAR3 heteromer-mediated mechanism that was lost upon the knockout of either receptor subunit. This is further corroborated by our detection of FFAR2-FFAR3 heteromers in monocytes and macrophages (Fig. 1), which belong to the bone marrow–derived immune cell subset that has been associated with the FFAR2- and FFAR3-mediated colitis phenotype (10, 14). In monocytes, the heteromerization of FFAR2-FFAR3 enabled p38 phosphorylation during acetate stimulation (Fig. 5), a key intracellular signaling protein for inflammatory function including that of monocytes (54). The observation of heteromer-specific pathways in physiologic processes would be indicative of heteromer-mediated function, as was proposed by the International Union of Basic and Clinical Pharmacology (55). It is perhaps no coincidence that the same acetate treatment is associated with the inhibition of p38 phosphorylation in colon epithelial cells (14), which are negative for FFAR2-FFAR3 heteromers (Fig. 1) despite being positive for both FFAR2 and FFAR3

Downloaded from www.fasebj.org by (137.132.3.10) on January 23, 2018. The FASEB Journal Vol. 32, No. 1, pp. 289-303.

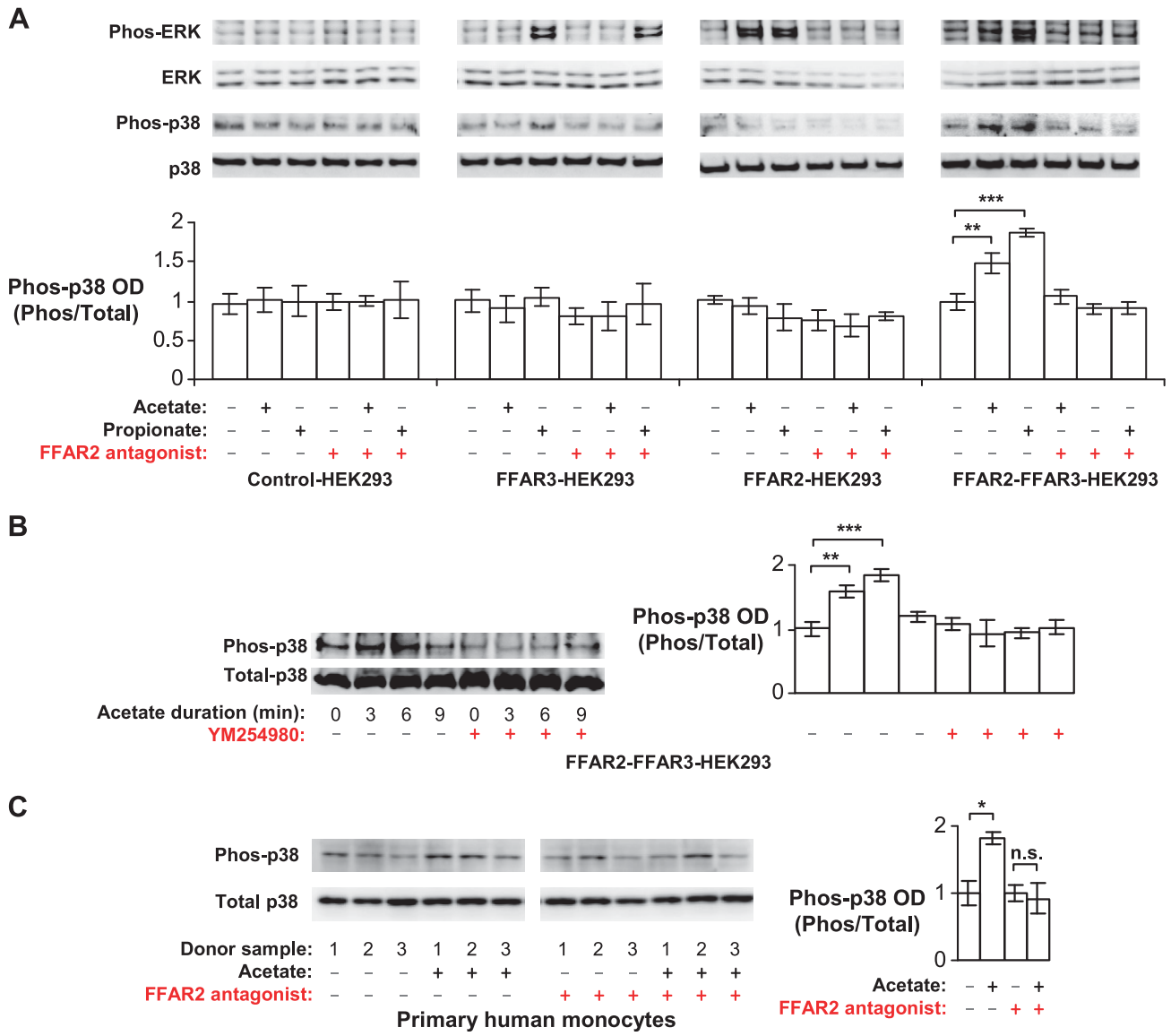

Figure 5. FFAR2-FFAR3 heteromerization enables p38 phosphorylation in HEK293 and monocytes. This effect was abolished by FFAR2 antagonism and $G_{\alpha q}$ inhibition. *A*, *B*) HEK293 cell lines that stably express FFAR3, FFAR2, or both (*i.e.*, control-, FFAR3-, FFAR2- and FFAR2-FFAR3-HEK293) were stimulated with 10 mM acetate or 10 mM propionate for 6 min (*A*) or indicated times (*B*). Western blots are representative of 3 independent experiments. Optical density (OD) measurements of 3 independent experiments are shown (means ± SD). *C*) Monocytes were stimulated with 10 mM acetate for 3 min. Western blot displays samples from 3 different donors. Corresponding OD is shown as means ± SD; $n = 3$. Vehicle control has been arbitrarily assigned value of 1. Two-tailed Welch's *t* test was used to determine statistical significance. $^*P < 0.05$, $^{**}P < 0.01$, $^{***}P < 0.001$.

expression (27–29). These findings suggest that SCFA stimulation of FFAR2/3 may have markedly different downstream signaling depending on whether FFAR2-FFAR3 heteromerization has occurred, such as the FFAR2-FFAR3 heteromer-mediated p38 activation in monocytes *vs.* the possible FFAR2/3 homomer-mediated inhibition of p38 in colon epithelial cells.

FFAR2-FFAR3 heteromer-mediated signaling may predominate over homomer-mediated pathways

Signaling from the FFAR2-FFAR3 heteromer may predominate over homomer-mediated pathways during the coexpression of both receptors. This is inferred from the observation that none of the characteristics associated with homomeric FFAR2/3 signaling is observed during coexpression. For example, FFAR2-FFAR2-HEK293 cells failed to inhibit cAMP, a pathway that is activated in cells that express only homomeric FFAR2 and FFAR3 (FFAR2-HEK293 and FFAR3-HEK293) (Fig. 3*F*). Insensitivity to FFAR2 antagonist and $G_{\alpha q}$ inhibitor treatment during acetate induction of β-arrestin-2 recruitment (Fig. 4*D*) and ERK1/2 signaling (Fig. 5*A, B*) were also observed in homomeric FFAR3tTa-HEK293 and FFAR3-HEK293, but not in heteromeric FFAR3tTa-FFAR2-HEK293 and FFAR2-FFAR3-HEK293. One would expect to observe at least some homomer-specific signaling phenotypes if significant populations of homomeric FFAR2 or FFAR3

Downloaded from www.fasebj.org by (137.132.3.10) on January 23, 2018. The FASEB Journal Vol. 32, No. 1, pp. 289-303.

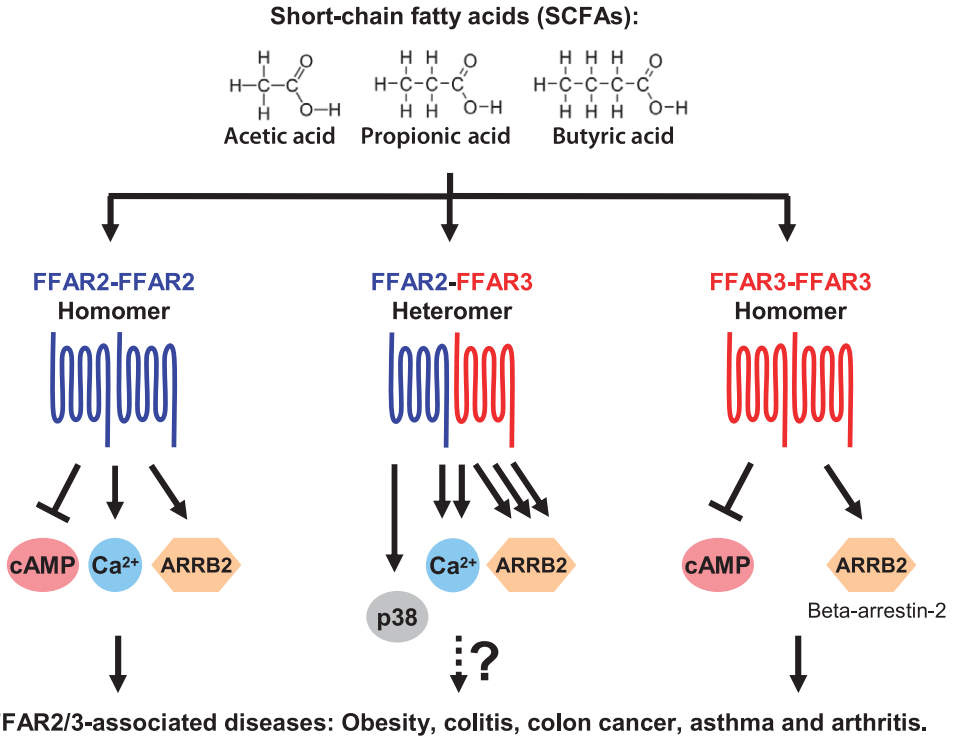

Figure 6. FFAR2-FFAR3 heteromer displays signaling that is distinct from parent homomers. Heteromer displays enhanced intracellular Ca^{2+} signaling (1.5-fold increase relative to homomeric FFAR2) and β-arrestin-2 recruitment (30-fold increase relative to homomeric FFAR3) while losing ability to inhibit cAMP production. These heteromer-mediated enhancements were attenuated by FFAR2 antagonism (CATPB), $G_{\alpha q}$ inhibition (YM254890), or $G_{\alpha i}$ inhibition (pertussis toxin). Heteromerization also enabled p38 phosphorylation *via* CATPB- and YM254890-sensitive mechanism.

exist during coexpression, which was not the case. The heteromeric form being predominant over the homomeric form of a GPCR receptor pairing has been previously described for the A_1R-$A_{2A}R$ heteromer, which was found in preponderance over homomeric A_1R and $A_{2A}R$ during the coexpression of both receptors (56). Thus, future studies may wish to explore whether SCFA signaling is indeed predominantly FFAR2-FFAR3 heteromer mediated, which would have significant implications for drug design.

FFAR2-FFAR3 heteromer may mediate induction of p38 phosphorylation in monocytes

Our results suggest that the FFAR2-FFAR3 heteromer is responsible for the induction of p38 phosphorylation observed during acetate treatment of inflammatory monocytes (29). First, only heteromeric FFAR2-FFAR3-HEK293 and not homomeric FFAR2/3-HEK293 displayed the ability to phosphorylate p38 during acetate or propionate stimulation (Fig. 5*A*). Second, when both receptors are expressed in HEK293 cells, the SCFA-induced signaling was predominantly FFAR2-FFAR3 heteromer mediated over homomer mediated, suggesting that the response in human monocytes may also be predominantly mediated by the FFAR2-FFAR3 heteromer observed (Fig. 1*A*). Third, acetate-induced p38 phosphorylation in monocytes was abolished by $G_{\alpha q}$ inhibition (29) and by FFAR2 antagonism (Fig. 5C), which matches heteromeric FFAR2-FFAR3-HEK293 cells (Fig. 5*A, B*). Last, because both FFAR2- and FFAR3-specific agonists were found to induce p38 phosphorylation in monocytes (29), only the FFAR2-FFAR3 heteromer would be activated by both agonists.

Future directions

While our study offers a first glimpse into the formation of a FFAR2-FFAR3 heteromer, much of its functions and roles remain to be discovered. First, further studies are required to explore the involvement of heteromer in physiologic functions and whether receptor heteromerization is necessary for the unique signaling or function. Confirming the role of the heteromer *in vivo* remains challenging, as FFAR2/3-knockout mice are likely to lose both homomer- and heteromer-dependent functions. New tools will need to be developed. A potential strategy is to develop a short peptide that would disrupt the interaction between FFAR2 and FFAR3. This strategy was successfully used for the D_1-D_2 dopamine heteromer (26). Another strategy is to identify and mutate the residues involved in the FFAR2-FFAR3 interaction to generate mutants that do not heteromerize. Noninteracting mutants may also serve as the ideal negative control for *in vitro* assays, such as the BiFC assay. Second, the PLA (Fig. 1) and BiFC (Fig. 2) studies we used did not reveal the stoichiometry of the FFAR2-FFAR3 heteromer, the FFAR2 homomer, and the FFAR3 homomer. Using single-particle imaging and tracking of fluorescent protein–tagged receptors, a previous study had concluded that the predominant stoichiometry of heterologously expressed A_1R-$A_{2A}R$ heteromers is 2:2—that is, a dimer of dimers (tetramer) (56). A similar strategy may be used to elucidate the stoichiometry of FFAR2-FFAR3. Third, additional experiments using $G_{\alpha q}$- and $G_{\alpha i}$-deficient mutants may further elucidate the G-protein coupling of the FFAR2-FFAR3 heteromer. We cannot rule out the possibility that the inhibitors used in this study may have off-target effects. For example, a close analog of YM254890,

Downloaded from www.fasebj.org by (137.132.3.10) on January 23, 2018. The FASEB Journal Vol. 32, No. 1, pp. 289-303.

UBO-QIC (FR900359), was found to inhibit the Ca^{2+} mobilization induced by the βγ subunits released from $G_{\alpha i}$ (57). Last, not much is known about the mechanism by which heteromerization alters FFAR2 and FFAR3 signaling. Heteromerization may increase affinity or affect ligand binding sites, which can be probed with fluorescent tracers. A fluorescent tracer based on a known azetidine FFAR2 antagonist has been described (58). Fluorescent tracers based on FFAR2 and FFAR3 agonists will need to be developed. Isotopic labeling approaches can be used because it may be challenging to fluorescently tag the relatively small-size endogenous SCFA agonists (acetate, propionate, and butyrate).

FFAR2-FFAR3 heteromer as a novel drug target

The discovery of the heteromer allows for the development of a new generation of more potent drugs that target heteromer-specific pathways. For example, heteromer-specific drugs should theoretically only activate Ca^{2+} signaling without inhibiting cAMP, while drugs that activate homomeric FFAR2/3 would indiscriminately activate both pathways. Multiple FFAR2/3 functions, such as inflammatory p38 signaling and enhanced β-arrestin-2 recruitment, are mediated by the heteromer, and hence only drugs targeting the heteromer will activate these pathways. Such FFAR2-FFAR3 heteromer-specific drugs cannot be identified with the assays currently being used, which express FFAR2/3 in homomeric form (30, 32, 53). Instead, assays that use the FFAR2-FFAR3 heteromer are required. Many of the FFAR2-FFAR3 heteromer assays established in this study, such as the cAMP-Glo assay, the NFAT luciferase reporter assay, and the Tango assay, with the latter using plasmids sourced from the PRESTO-Tango system (41), are readily scalable for high-throughput screening or rational drug design and testing.

CONCLUSIONS

We have demonstrated that FFAR2 and FFAR3 interact to form a heteromer with distinct signaling. Further studies are required to investigate the possibility that the disease phenotypes (*e.g.*, obesity, colitis, colon cancer, asthma, and arthritis) observed in mice upon the single knockout of either FFAR2 or FFAR3 (3–20) may be due to the accompanying loss of the heteromer and its unique signaling output. The heteromer would thus be a novel drug target for the treatment of these diseases. FJ

ACKNOWLEDGMENTS

The authors gratefully acknowledge the kind gifts of YM254890 from Taiho Pharmaceutical (Tokyo, Japan); CATPB from S. Kim (Korean Research Institute of Bioscience and Biotechnology, Daejeon, South Korea); expression plasmids, hFFA2-eYFP and hFFA3-eYFP in pcDNA5/FRT/TO from G. Milligan (University of Glasgow, Glasgow, United Kingdom); pBiFC-VN155(I152L) and pBiFC-VC155 plasmids from C.-D. Hu (27097 and 22011; Addgene; Purdue University, West Lafayette, IN, USA); FFA2-Tango, FFA3-Tango, and P2RY1-Tango plasmids (66281, 66282, 66468; Addgene) and HTLA cells from B. Roth (University of North Carolina at Chapel Hill, Chapel Hill, NC, USA). This work was supported by grants from the National Medical Research Council (NMRC/CBRG/0055/2013) and the Ministry of Education (MoE 2013-T2-2-007 and MoE R-154-000-A31-114 to J.L.D., and MoE 2015-T2-1-122 to M.W.). The authors declare no conflicts of interest.

AUTHOR CONTRIBUTIONS

Z. Ang designed and performed research; D. Xiong performed the FRET and calcium measurements; D. Xiong and M. Wu contributed new reagents or analytic tools; and Z. Ang, D. Xiong, M. Wu, and J.L. Ding analyzed the data and wrote the article.

REFERENCES

1. Brown, A. J., Goldsworthy, S. M., Barnes, A. A., Eilert, M. M., Tcheang, L., Daniels, D., Muir, A. I., Wigglesworth, M. J., Kinghorn, I., Fraser, N. J., Pike, N. B., Strum, J. C., Steplewski, K. M., Murdock, P. R., Holder, J. C., Marshall, F. H., Szekeres, P. G., Wilson, S., Ignar, D. M., Foord, S. M., Wise, A., and Dowell, S. J. (2003) The Orphan G protein–coupled receptors GPR41 and GPR43 are activated by propionate and other short chain carboxylic acids. *J. Biol. Chem.* **278**, 11312–11319
2. Le Poul, E., Loison, C., Struyf, S., Springael, J.-Y., Lannoy, V., Decobecq, M.-E., Brezillon, S., Dupriez, V., Vassart, G., Van Damme, J., Parmentier, M., and Detheux, M. (2003) Functional characterization of human receptors for short chain fatty acids and their role in polymorphonuclear cell activation. *J. Biol. Chem.* **278**, 25481–25489
3. Tang, C., Ahmed, K., Gille, A., Lu, S., Gröne, H.-J., Tunaru, S., and Offermanns, S. (2015) Loss of FFA2 and FFA3 increases insulin secretion and improves glucose tolerance in type 2 diabetes. *Nat. Med.* **21**, 173–177
4. Ge, H., Li, X., Weiszmann, J., Wang, P., Baribault, H., Chen, J.-L., Tian, H., and Li, Y. (2008) Activation of G protein–coupled receptor 43 in adipocytes leads to inhibition of lipolysis and suppression of plasma free fatty acids. *Endocrinology* **149**, 4519–4526
5. Bjursell, M., Admyre, T., Göransson, M., Marley, A. E., Smith, D. M., Oscarsson, J., and Bohlooly-Y, M. (2011) Improved glucose control and reduced body fat mass in free fatty acid receptor 2–deficient mice fed a high-fat diet. *Am. J. Physiol. Endocrinol. Metab.* **300**, E211–E220
6. Tolhurst, G., Heffron, H., Lam, Y. S., Parker, H. E., Habib, A. M., Diakogiannaki, E., Cameron, J., Grosse, J., Reimann, F., and Gribble, F. M. (2012) Short-chain fatty acids stimulate glucagon-like peptide-1 secretion *via* the G-protein-coupled receptor FFAR2. *Diabetes* **61**, 364–371
7. Kimura, I., Ozawa, K., Inoue, D., Imamura, T., Kimura, K., Maeda, T., Terasawa, K., Kashihara, D., Hirano, K., Tani, T., Takahashi, T., Miyauchi, S., Shioi, G., Inoue, H., and Tsujimoto, G. (2013) The gut microbiota suppresses insulin-mediated fat accumulation *via* the short-chain fatty acid receptor GPR43. *Nat. Commun.* **4**, 1829
8. McNelis, J. C., Lee, Y. S., Mayoral, R., van der Kant, R., Johnson, A. M. F., Wollam, J., and Olefsky, J. M. (2015) GPR43 potentiates beta cell function in obesity. *Diabetes* **64**, 3203–3217
9. Priyadarshini, M., Villa, S. R., Fuller, M., Wicksteed, B., Mackay, C. R., Alquier, T., Poitout, V., Mancebo, H., Mirmira, R. G., Gilchrist, A., and Layden, B. T. (2015) An acetate-specific GPCR, FFAR2, regulates insulin secretion. *Mol. Endocrinol.* **29**, 1055–1066
10. Maslowski, K. M., Vieira, A. T., Ng, A., Kranich, J., Sierro, F., Yu, D., Schilter, H. C., Rolph, M. S., Mackay, F., Artis, D., Xavier, R. J., Teixeira, M. M., and Mackay, C. R. (2009) Regulation of inflammatory responses by gut microbiota and chemoattractant receptor GPR43. *Nature* **461**, 1282–1286
11. Sina, C., Gavrilova, O., Förster, M., Till, A., Derer, S., Hildebrand, F., Raabe, B., Chalaris, A., Scheller, J., Rehmann, A., Franke, A., Ott, S., Häsler, R., Nikolaus, S., Fölsch, U. R., Rose-John, S., Jiang, H.-P., Li, J., Schreiber, S., and Rosenstiel, P. (2009) G protein–coupled receptor

Downloaded from www.fasebj.org by (137.132.3.10) on January 23, 2018. The FASEB Journal Vol. 32, No. 1, pp. 289-303.

43 is essential for neutrophil recruitment during intestinal inflammation. *J. Immunol.* **183**, 7514–7522
12. Smith, P. M., Howitt, M. R., Panikov, N., Michaud, M., Gallini, C. A., Bohlooly-Y, M., Glickman, J. N., and Garrett, W. S. (2013) The microbial metabolites, short-chain fatty acids, regulate colonic Treg cell homeostasis. *Science* **341**, 569–573
13. Masui, R., Sasaki, M., Funaki, Y., Ogasawara, N., Mizuno, M., Iida, A., Izawa, S., Kondo, Y., Ito, Y., Tamura, Y., Yanamoto, K., Noda, H., Tanabe, A., Okaniwa, N., Yamaguchi, Y., Iwamoto, T., and Kasugai, K. (2013) G protein–coupled receptor 43 moderates gut inflammation through cytokine regulation from mononuclear cells. *Inflamm. Bowel Dis.* **19**, 2848–2856
14. Kim, M. H., Kang, S. G., Park, J. H., Yanagisawa, M., and Kim, C. H. (2013) Short-chain fatty acids activate GPR41 and GPR43 on intestinal epithelial cells to promote inflammatory responses in mice. *Gastroenterology* **145**, 396–406.e1–e10
15. Macia, L., Tan, J., Vieira, A. T., Leach, K., Stanley, D., Luong, S., Maruya, M., Ian McKenzie, C., Hijikata, A., Wong, C., Binge, L., Thorburn, A. N., Chevalier, N., Ang, C., Marino, E., Robert, R., Offermanns, S., Teixeira, M. M., Moore, R. J., Flavell, R. A., Fagarasan, S., and Mackay, C. R. (2015) Metabolite-sensing receptors GPR43 and GPR109A facilitate dietary fibre–induced gut homeostasis through regulation of the inflammasome. *Nat. Commun.* **6**, 6734
16. Vieira, A. T., Macia, L., Galvão, I., Martins, F. S., Canesso, M. C. C., Amaral, F. A., Garcia, C. C., Maslowski, K. M., De Leon, E., Shim, D., Nicoli, J. R., Harper, J. L., Teixeira, M. M., and Mackay, C. R. (2015) A role for gut microbiota and the metabolite-sensing receptor GPR43 in a murine model of gout. *Arthritis Rheumatol.* **67**, 1646–1656
17. Sivaprakasam, S., Gurav, A., Paschall, A. V., Coe, G. L., Chaudhary, K., Cai, Y., Kolhe, R., Martin, P., Browning, D., Huang, L., Shi, H., Sifuentes, H., Vijay-Kumar, M., Thompson, S. A., Munn, D. H., Mellor, A., McGaha, T. L., Shiao, P., Cutler, C. W., Liu, K., Ganapathy, V., Li, H., and Singh, N. (2016) An essential role of Ffar2 (Gpr43) in dietary fibre-mediated promotion of healthy composition of gut microbiota and suppression of intestinal carcinogenesis. *Oncogenesis* **5**, e238
18. Natarajan, N., Hori, D., Flavahan, S., Steppan, J., Flavahan, N. A., Berkowitz, D. E., and Pluznick, J. L. (2016) Microbial short chain fatty acid metabolites lower blood pressure *via* endothelial G-protein coupled receptor 41. *Physiol. Genomics* **48**, 826–834
19. Trompette, A., Gollwitzer, E. S., Yadava, K., Sichelstiel, A. K., Sprenger, N., Ngom-Bru, C., Blanchard, C., Junt, T., Nicod, L. P., Harris, N. L., and Marsland, B. J. (2014) Gut microbiota metabolism of dietary fiber influences allergic airway disease and hematopoiesis. *Nat. Med.* **20**, 159–166
20. Sergeev, E., Hansen, A. H., Pandey, S. K., MacKenzie, A. E., Hudson, B. D., Ulven, T., and Milligan, G. (2016) Non-equivalence of key positively charged residues of the free fatty acid 2 receptor in the recognition and function of agonist *versus* antagonist ligands. *J. Biol. Chem.* **291**, 303–317
21. Ng, J., Rashid, A. J., So, C. H., O'Dowd, B. F., and George, S. R. (2010) Activation of calcium/calmodulin-dependent protein kinase IIalpha in the striatum by the heteromeric D1-D2 dopamine receptor complex. *Neuroscience* **165**, 535–541
22. Rodríguez-Ruiz, M., Moreno, E., Moreno-Delgado, D., Navarro, G., Mallol, J., Cortés, A., Lluís, C., Canela, E. I., Casadó, V., McCormick, P. J., and Franco, R. (2016) Heteroreceptor complexes formed by dopamine D1, histamine H3, and *N*-methyl-D-aspartate glutamate receptors as targets to prevent neuronal death in Alzheimer's disease. *Mol. Neurobiol.* **54**, 4537–4550
23. Rozenfeld, R., and Devi, L. A. (2007) Receptor heterodimerization leads to a switch in signaling: beta-arrestin2-mediated ERK activation by mu-delta opioid receptor heterodimers. *FASEB J.* **21**, 2455–2465
24. Ganguly, S., Clayton, A. H. A., and Chattopadhyay, A. (2011) Organization of higher-order oligomers of the serotonin$_1$(A) receptor explored utilizing homo-FRET in live cells. *Biophys. J.* **100**, 361–368
25. Armando, S., Quoyer, J., Lukashova, V., Maiga, A., Percherancier, Y., Heveker, N., Pin, J.-P., Prézeau, L., and Bouvier, M. (2014) The chemokine CXC*4* and CC2 receptors form homo- and heterooligomers that can engage their signaling G-protein effectors and βarrestin. *FASEB J.* **28**, 4509–4523
26. Pei, L., Li, S., Wang, M., Diwan, M., Anisman, H., Fletcher, P. J., Nobrega, J. N., and Liu, F. (2010) Uncoupling the dopamine D1-D2 receptor complex exerts antidepressant-like effects. *Nat. Med.* **16**, 1393–1395
27. Karaki, S., Tazoe, H., Hayashi, H., Kashiwabara, H., Tooyama, K., Suzuki, Y., and Kuwahara, A. (2008) Expression of the short-chain fatty acid receptor, GPR43, in the human colon. *J. Mol. Histol.* **39**, 135–142
28. Tazoe, H., Otomo, Y., Karaki, S., Kato, I., Fukami, Y., Terasaki, M., and Kuwahara, A. (2009) Expression of short-chain fatty acid receptor GPR41 in the human colon. *Biomed. Res.* **30**, 149–156
29. Ang, Z., Er, J. Z., Tan, N. S., Lu, J., Liou, Y.-C., Grosse, J., and Ding, J. L. (2016) Human and mouse monocytes display distinct signalling and cytokine profiles upon stimulation with FFAR2/FFAR3 short-chain fatty acid receptor agonists. *Sci. Rep.* **6**, 34145
30. Brantis, C. E., Ooms, F., Bernard, J. (2011) Novel amino acid derivatives and their use as GPR43 receptor modulators. Patent WO/2011/092284
31. Park, B.-O., Kim, S. H., Kong, G. Y., Kim, D. H., Kwon, M. S., Lee, S. U., Kim, M.-O., Cho, S., Lee, S., Lee, H.-J., Han, S.-B., Kwak, Y. S., Lee, S. B., and Kim, S. (2016) Selective novel inverse agonists for human GPR43 augment GLP-1 secretion. *Eur. J. Pharmacol.* **771**, 1–9
32. Wang, Y., Jiao, X., Kayser, F., Liu, J., Wang, Z., Wanska, M., Greenberg, J., Weiszmann, J., Ge, H., Tian, H., Wong, S., Schwandner, R., Lee, T., and Li, Y. (2010) The first synthetic agonists of FFA2: discovery and SAR of phenylacetamides as allosteric modulators. *Bioorg. Med. Chem. Lett.* **20**, 493–498
33. Leonard, J. N., Chu, Z. L., Bruce, M. A., Boatman, P. D. (2008) Gpr41 and modulators thereof for the treatment of insulin-related disorders. Patent US 20080312277 A1
34. Ang, Z., Er, J. Z., and Ding, J. L. (2015) The short-chain fatty acid receptor GPR43 is transcriptionally regulated by XBP1 in human monocytes. *Sci. Rep.* **5**, 8134
35. Pfaffl, M. W. (2001) A new mathematical model for relative quantification in real-time RT-PCR. *Nucleic Acids Res.* **29**, e45
36. Pfaffl, M. W., Horgan, G. W., and Dempfle, L. (2002) Relative expression software tool (REST) for group-wise comparison and statistical analysis of relative expression results in real-time PCR. *Nucleic Acids Res.* **30**, e36
37. Kodama, Y., and Hu, C.-D. (2010) An improved bimolecular fluorescence complementation assay with a high signal-to-noise ratio. *Biotechniques* **49**, 793–805
38. Stoddart, L. A., Smith, N. J., Jenkins, L., Brown, A. J., and Milligan, G. (2008) Conserved polar residues in transmembrane domains V, VI, and VII of free fatty acid receptor 2 and free fatty acid receptor 3 are required for the binding and function of short chain fatty acids. *J. Biol. Chem.* **283**, 32913–32924
39. Tian, L., Hires, S. A., Mao, T., Huber, D., Chiappe, M. E., Chalasani, S. H., Petreanu, L., Akerboom, J., McKinney, S. A., Schreiter, E. R., Bargmann, C. I., Jayaraman, V., Svoboda, K., and Looger, L. L. (2009) Imaging neural activity in worms, flies and mice with improved GCaMP calcium indicators. *Nat. Methods* **6**, 875–881
40. Gouell, S., Hsaio, K. Monitoring the activity of G protein–coupled receptors (GPCR) modulated by lipid or free fatty acid agonists. (2009) Accessed August 30, 2017, at: https://www.promega.com/resources/pubhub/cellnotes/monitoring-the-activity-of-gpcrs–modulated-by-lipids-or-free-fatty-acids/
41. Kroeze, W. K., Sassano, M. F., Huang, X.-P., Lansu, K., McCorvy, J. D., Giguère, P. M., Sciaky, N., and Roth, B. L. (2015) PRESTO-Tango as an open-source resource for interrogation of the druggable human GPCRome. *Nat. Struct. Mol. Biol.* **22**, 362–369
42. Barnea, G., Strapps, W., Herrada, G., Berman, Y., Ong, J., Kloss, B., Axel, R., and Lee, K. J. (2008) The genetic design of signaling cascades to record receptor activation. *Proc. Natl. Acad. Sci. USA* **105**, 64–69
43. Rico, A. J., Dopeso-Reyes, I. G., Martínez-Pinilla, E., Sucunza, D., Pignataro, D., Roda, E., Marín-Ramos, D., Labandeira-García, J. L., George, S. R., Franco, R., and Lanciego, J. L. (2017) Neurochemical evidence supporting dopamine D1-D2 receptor heteromers in the striatum of the long-tailed macaque: changes following dopaminergic manipulation. *Brain Struct. Funct.* **222**, 1767–1784
44. Karpova, T. S., Baumann, C. T., He, L., Wu, X., Grammer, A., Lipsky, P., Hager, G. L., and McNally, J. G (2003) Fluorescence resonance energy transfer from cyan to yellow fluorescent protein detected by acceptor photobleaching using confocal microscopy and a single laser. *J. Microsc.* **209**, 56–70
45. Stoddart, L. A. (2007) *Investigation of the Function, Pharmacology and Oligomerisation of GPR40, GPR41 and GPR43*, University of Glasgow, Glasgow, United Kingdom

Downloaded from www.fasebj.org by (137.132.3.10) on January 23, 2018. The FASEB Journal Vol. 32, No. 1, pp. 289-303.

46. Joost, P., and Methner, A. (2002) Phylogenetic analysis of 277 human G-protein-coupled receptors as a tool for the prediction of orphan receptor ligands. *Genome Biol.* **3**, RESEARCH0063
47. Choi, R. C. Y., Simon, J., Tsim, K. W. K., and Barnard, E. A. (2008) Constitutive and agonist-induced dimerizations of the P2Y1 receptor: relationship to internalization and scaffolding. *J. Biol. Chem.* **283**, 11050–11063
48. Jacobsen, S. E., Ammendrup-Johnsen, I., Jansen, A. M., Gether, U., Madsen, K. L., and Bräuner-Osborne, H. (2017) The GPRC6A receptor displays constitutive internalization and sorting to the slow recycling pathway. *J. Biol. Chem.* **292**, 6910–6926
49. Levoye, A., Zwier, J. M., Jaracz-Ros, A., Klipfel, L., Cottet, M., Maurel, D., Bdioui, S., Balabanian, K., Prézeau, L., Trinquet, E., Durroux, T., and Bachelerie, F. (2015) A broad G protein–coupled receptor internalization assay that combines SNAP-tag labeling, diffusion-enhanced resonance energy transfer, and a highly emissive terbium cryptate. *Front. Endocrinol. (Lausanne)* **6**, 167
50. Hudson, B. D., Christiansen, E., Tikhonova, I. G., Grundmann, M., Kostenis, E., Adams, D. R., Ulven, T., and Milligan, G. (2012) Chemically engineering ligand selectivity at the free fatty acid receptor 2 based on pharmacological variation between species orthologs. *FASEB J.* **26**, 4951–4965
51. Lee, S. U., In, H. J., Kwon, M. S., Park, B. O., Jo, M., Kim, M.-O., Cho, S., Lee, S., Lee, H.-J., Kwak, Y. S., and Kim, S. (2013) β-Arrestin 2 mediates G protein–coupled receptor 43 signals to nuclear factor-κB. *Biol. Pharm. Bull.* **36**, 1754–1759
52. Vinolo, M. A. R., Ferguson, G. J., Kulkarni, S., Damoulakis, G., Anderson, K., Bohlooly-Y, M., Stephens, L., Hawkins, P. T., and Curi, R. (2011) SCFAs induce mouse neutrophil chemotaxis through the GPR43 receptor. *PLoS One* **6**, e21205
53. Takasaki, J., Saito, T., Taniguchi, M., Kawasaki, T., Moritani, Y., Hayashi, K., and Kobori, M. (2004) A novel Galphaq/11-selective inhibitor. *J. Biol. Chem.* **279**, 47438–47445
54. Herlaar, E., and Brown, Z. (1999) p38 MAPK signalling cascades in inflammatory disease. *Mol. Med. Today* **5**, 439–447
55. Pin, J.-P., Neubig, R., Bouvier, M., Devi, L., Filizola, M., Javitch, J. A., Lohse, M. J., Milligan, G., Palczewski, K., Parmentier, M., and Spedding, M. (2007) International Union of Basic and Clinical Pharmacology. LXVII. Recommendations for the recognition and nomenclature of G protein–coupled receptor heteromultimers. *Pharmacol. Rev.* **59**, 5–13
56. Navarro, G., Cordomí, A., Zelman-Femiak, M., Brugarolas, M., Moreno, E., Aguinaga, D., Perez-Benito, L., Cortés, A., Casadó, V., Mallol, J., Canela, E. I., Lluís, C., Pardo, L., García-Sáez, A. J., McCormick, P. J., and Franco, R. (2016) Quaternary structure of a G-protein-coupled receptor heterotetramer in complex with Gi and Gs. *BMC Biol.* **14**, 26
57. Gao, Z.-G., and Jacobson, K. A. (2016) On the selectivity of the Gαq inhibitor UBO-QIC: a comparison with the Gαi inhibitor pertussis toxin. *Biochem. Pharmacol.* **107**, 59–66
58. Hansen, A. H., Sergeev, E., Pandey, S. K., Hudson, B. D., Christiansen, E., Milligan, G., and Ulven, T. (2017) Development and characterization of a fluorescent tracer for the free fatty acid receptor 2 (FFA2/GPR43). *J. Med. Chem.* **60**, 5638–5645

Received for publication March 23, 2017.
Accepted for publication August 28, 2017.

Downloaded from www.fasebj.org by (137.132.3.10) on January 23, 2018. The FASEB Journal Vol. 32, No. 1, pp. 289-303.